JGR Solid Earth

RESEARCH ARTICLE
10.1029/2024JB029516

Widespread D″ Anisotropy Beneath North America and the Northeastern Pacific and Implications for Upper Mantle Anisotropy Measurements

Jonathan Wolf[1,2,3], Daniel A. Frost[4], Alexia Brewster[4], Maureen D. Long[1], Ed Garnero[5], and John D. West[5]

[1]Department of Earth and Planetary Sciences, Yale University, New Haven, CT, USA, [2]Department of Earth and Planetary Science, University of California, Berkeley, Berkeley, CA, USA, [3]Miller Institute for Basic Scienc, Berkeley, CA, USA, [4]School of the Earth, Ocean and Environment, University of South Carolina, Columbia, SC, USA, [5]School of Earth and Space Exploration, Arizona State University, Tempe, AZ, USA

Abstract Observations of seismic waves that have passed through the Earth's lowermost mantle provide insight into deep mantle structure and dynamics, often on relatively small spatial scales. Here we use SKS, S2KS, S3KS, and PKS signals recorded across a large region including the United States, Mexico, and Central America to study the deepest mantle beneath large swaths of North America and the northeastern Pacific Ocean. These phases are enhanced via beamforming and then used to investigate polarization- and propagation direction-dependent shear wave speeds (seismic anisotropy). A differential splitting approach enables us to robustly identify contributions from D″ anisotropy. Our results show strong seismic anisotropy in approximately half of our study region, indicating that D″ anisotropy may be more prevalent than commonly thought. In some regions, the anisotropy may be induced by flow driven by sinking cold slabs, and in other, more compact regions, by upwelling flow. Measured splitting due to lowermost mantle anisotropy is sufficiently strong to be non-negligible in interpretations of SKS splitting due to upper mantle anisotropy in certain regions, which may prompt future re-evaluations of upper mantle anisotropy beneath North and Central America.

Plain Language Summary Earthquakes emit seismic waves that travel through Earth's deep interior. In some parts of Earth, the speed of these waves depends on their vibrational directions. In these cases, the material they travel through can be described as seismically anisotropic. Such seismic anisotropy is often caused by material deformation due to convective flow in Earth's interior. We show in this work that Earth's mantle beneath North America and the northeastern Pacific Ocean is seismically anisotropic in many places just above its boundary with the core at a depth of ~2900 km. In some of these places, the deformation may be caused by sinking subducted slabs, upwelling flow, or changes in horizontal flow at the mantle's lower boundary layer. We additionally show that potential contributions from the lowermost mantle anisotropy cannot always be neglected when measuring seismic anisotropy in other parts of the mantle.

Key Points:

- We infer D″ seismic anisotropy beneath North America and parts of the Pacific Ocean from beamformed SKS, S2KS, S3KS, and PKS data
- We find widespread seismic anisotropy in the deepest mantle, likely induced by a variety of different convective flow regimes
- The influence of the deepest mantle on SKS (usually used to infer upper mantle anisotropy) is non-negligible in some regions

Supporting Information:

Supporting Information may be found in the online version of this article.

Correspondence to:

J. Wolf,
jonathan.wolf@berkeley.edu

Citation:

Wolf, J., Frost, D. A., Brewster, A., Long, M. D., Garnero, E., & West, J. D. (2024). Widespread D″ anisotropy beneath North America and the northeastern Pacific and implications for upper mantle anisotropy measurements. *Journal of Geophysical Research: Solid Earth*, *129*, e2024JB029516. https://doi.org/10.1029/2024JB029516

Received 13 MAY 2024
Accepted 14 OCT 2024

Author Contributions:

Conceptualization: Jonathan Wolf, Daniel A. Frost, Maureen D. Long, Ed Garnero
Data curation: Jonathan Wolf, Daniel A. Frost, Alexia Brewster, John D. West
Formal analysis: Jonathan Wolf, Daniel A. Frost
Funding acquisition: Daniel A. Frost, Maureen D. Long, Ed Garnero
Investigation: Jonathan Wolf, Daniel A. Frost, Alexia Brewster
Methodology: Jonathan Wolf, Daniel A. Frost

1. Introduction

The dependence of seismic wave velocities on the propagation and/or polarization direction of the wave (seismic anisotropy) is typically an indicator of deformation in Earth's interior (e.g., Long & Becker, 2010; Romanowicz & Wenk, 2017; Wolf, Li, Long, & Garnero, 2024). Shear-wave splitting measurements (e.g., Asplet et al., 2023; Hansen et al., 2021; Liu et al., 2014; Meade et al., 2005; Niu & Perez, 2004; Wolf, Long, Li, & Garnero, 2023) and seismic tomography (e.g., Chang et al., 2015; French & Romanowicz, 2014; Panning & Romanowicz, 2006) reveal that strong seismic anisotropy can be found in Earth's upper mantle and crust, the bulk of the lower mantle is almost isotropic, and the lowermost few 100 km of the mantle (the D″ layer) exhibit seismic anisotropy of (on average) moderate strength (Figure 1a). This observation can be explained if upper and lowermost mantle materials deform via dislocation creep, which causes the alignment of mineral crystals and thus seismic anisotropy, while the bulk of the lower mantle is dominated by diffusion creep, which generally does not lead to anisotropy (e.g., Karato et al., 2008; Kocks et al., 2000; Montagner, 1998; Wenk & Houtte, 2004).

D″ anisotropy has been detected in many regional studies (e.g., Asplet et al., 2020, 2023; Lay & Young, 1991; Nowacki et al., 2010; Wolf, Long, & Frost, 2024), which usually have lateral resolution capabilities of 100s of kilometers, as well as via global inversions for radially anisotropic structure (Chang et al., 2015; French &

Project administration: Daniel A. Frost, Maureen D. Long, Ed Garnero
Resources: Daniel A. Frost, Maureen D. Long, Ed Garnero
Software: Jonathan Wolf, Daniel A. Frost
Supervision: Daniel A. Frost, Maureen D. Long, Ed Garnero
Validation: Jonathan Wolf, Daniel A. Frost
Visualization: Jonathan Wolf, Daniel A. Frost
Writing – original draft: Jonathan Wolf, Daniel A. Frost
Writing – review & editing: Jonathan Wolf, Daniel A. Frost, Maureen D. Long, Ed Garnero, John D. West

Romanowicz, 2014), which reliably resolve large-scale structures. The regional studies published to date use a variety of different techniques, some of which are more sensitive to lowermost mantle anisotropy than others (Wolf, Li, Long, & Garnero, 2024). Only a few of these studies (e.g., Reiss et al., 2019; Suzuki et al., 2021) investigate seismic anisotropy in relatively large geographic regions using a comprehensive methodology, thereby enabling detailed inferences on seismic anisotropy over a broad region. Such uniform investigations are important to infer how widespread seismic anisotropy in D″ is, and how strongly it can affect the splitting of seismic waveforms, including phases that are often used to study upper mantle anisotropy.

For measurements of upper mantle shear-wave splitting from *KS waves, which travel through the outer core as P waves and then convert to S upon re-entry in the mantle from the core (e.g., SKS, S2KS or PKS; see Figure 1b, inset), it is typically assumed that the lowermost mantle anisotropy contribution can be neglected (e.g., Liu et al., 2014; Savage, 1999; Silver & Chan, 1991; Wolf & Long, 2023; Yang et al., 2017). This is because D″ anisotropy is, on average, weaker than upper mantle anisotropy (Figure 1a); furthermore, *KS waves may have stronger sensitivity to upper mantle anisotropy (e.g., Sieminski et al., 2008). At the same time, differential splitting between pairs of *KS waves is often attributed to D″ anisotropy because the raypaths of *KS phases sample different portions of the lowermost mantle, while they are almost identical in the upper mantle (e.g., Niu & Perez, 2004; Tesoniero et al., 2020; Wang & Wen, 2004). This technique does have some challenges, because moderate differences in shear wave splitting can also be due to the slightly different upper mantle raypaths (e.g., Lin et al., 2014; Tesoniero et al., 2020) or to seismic noise (Wolf, Frost, et al., 2023). However, if certain precautions are followed (such as only interpreting splitting intensity differences >0.4), discrepant *KS splitting has been shown to be generally reliable as a tool for detecting lowermost mantle anisotropy (Tesoniero et al., 2020; Wolf et al., 2022).

One novel method that has been shown to reduce noise while averaging single-station splitting parameters involves a beamforming approach (Frost et al., 2024; Wolf, Frost, et al., 2023). Beamforming (e.g., Frost et al., 2020; Rost & Thomas, 2002, 2009) stacks seismograms of a seismic phase across neighboring seismic stations, taking into account the differential travel times to stations with different locations. The increased signal-to-noise ratios (SNRs) of beamformed data can enable the measurement of shear wave splitting from seismic phases that are not usually used for this purpose due to their typically low amplitudes in single-station seismograms, such as S3KS (Wolf, Frost, et al., 2023). Additionally, by suppressing uncorrelated noise, beamforming diminishes the effects of scattering due to small-scale structure close to the receiver, leading to a substantial reduction of overall measurement scattering (due to noise) for many commonly used *KS seismic phases (e.g., SKS, S2KS). Therefore, the measurement of *KS differential splitting using a beamforming approach is well-suited to both (a) provide constraints on lowermost mantle anisotropy in a broad region and (b) allow inferences on the influence of this lowermost mantle anisotropy on upper mantle measurements. Wolf, Frost, et al. (2023) developed the *KS beam splitting technique and presented a proof-of-concept application to a limited data set from North America; however, the technique has yet to be widely applied to study deep mantle anisotropy. Here we expand on the work of Wolf, Frost, et al. (2023) and apply differential *KS beam splitting to array data throughout North America, with the goal of providing a comprehensive view of D″ anisotropy beneath the region.

2. Methods

2.1. Data Selection and Beamforming

The lowermost mantle beneath North America and the northeastern Pacific Ocean represents an ideal application for differential *KS beam splitting measurements. This region features excellent data coverage, with the past installation of the dense Transportable Array (IRIS Transportable Array, 2003) across parts of this region and the good ray coverage for *KS waves from subduction zone earthquakes in the southwestern Pacific Ocean and South America (Figure 1b). Using single-station SKS-S2KS data, the presence of seismic anisotropy has been previously suggested for parts of this region, in particular beneath the northeastern Pacific Ocean (e.g., Asplet et al., 2020, 2023; Long, 2009; Wolf & Long, 2022) and the western United States (e.g., Lutz et al., 2020; Nowacki et al., 2010; Wolf, Li, Haws, & Long, 2024). However, these single-station measurements often showed different measurement results for adjacent raypaths, likely due to noise.

We focus on events over magnitude 6 within 100–140° from stations in Central America and North America. Events observed at 60 or more stations in either region are retained, resulting in 214 events. These data are

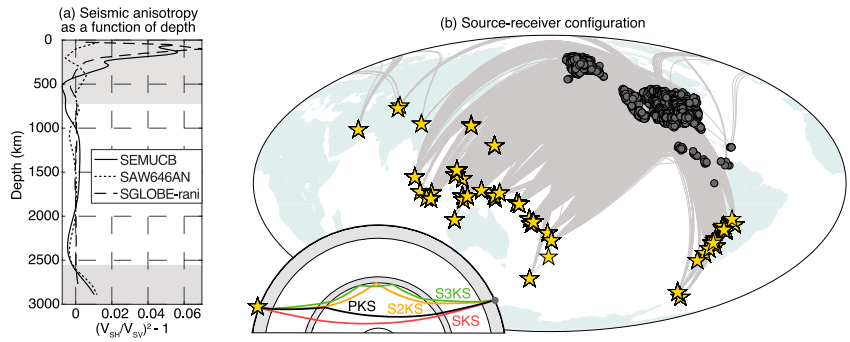

Figure 1. Distribution of seismic anisotropy in Earth and source-receiver configuration. (a) Radial anisotropy (described as the squared fraction of horizontal and vertical shear wave velocities minus 1) as a function of depth, as suggested by the tomography models SAW646AN (Megnin & Romanowicz, 2000), SEMUCB-WM1 (French & Romanowicz, 2014) and SGLOBE-rani (Chang et al., 2015) (see legend). The presence of substantial seismic anisotropy is indicated by gray shaded regions. (b) Source (yellow stars)—subarray (central station: gray circle) configuration used in this study. Gray lines indicate great circle raypaths. Inset: Cross-section of SKS, S2KS, S3KS, and PKS raypaths through Earth for an epicentral distance of 135° through isotropic PREM (Dziewonski & Anderson, 1981).

instrument deconvolved, horizontal components are rotated to radial and transverse directions, and seismograms are filtered between 0.02 and 0.25 Hz. Record sections of the radial component of each event are then manually inspected and events with clear *KS energy are retained, leaving 61 events (Table S1 in Supporting Information S1).

We apply the beamforming method of Frost et al. (2024) to this data. For each event, a 1 × 1 degree grid is set up across Central America and Alaska and at each grid point the nearest 5–20 stations are selected, forming a subarray (Figure 2). Subarrays with fewer than 5 stations are skipped. We attempt to form stacks for each of the following phases predicted to exist at that subarray according to PREM (Dziewonski & Anderson, 1981): SKS, S2KS, S3KS, and PKS. If more than one PKS wave arrives due to triplication, we analyze the first arriving wave.

Separately for the radial and transverse seismograms, and for each phase, data are windowed 40 s before and 40 s after the PREM-predicted arrival time. The optimal slowness and backazimuth for each phase is determined using gridsearch approach. We construct F-vespagrams (Frost et al., 2024) from individual F-traces (Blandford, 1974; Selby, 2008) themselves constructed for slownesses between 0 and 9 in 0.1 s/deg increments and backazimuths between −20 and 20° in 1° increments, measured relative to the great circle path. The optimal slowness and backazimuth are selected using the maximum F-value (coherence) in the vicinity of the predicted arrival of each phase. These optimal values are then used to construct linearly stacked beams so as to minimize waveform distortions, and enhance coherent signal, allowing the beams to be used for anisotropy calculations. This beam signal processing procedure is shown in Figure 2 using example S2KS seismograms recorded in southern Alaska (Figure 2a). In this example, the SNR of the beams (blue) is clearly enhanced compared to the single-station data (black; Figures 2b and 2c).

2.2. Shear-Wave Splitting Measurements

*KS seismic waves are SV-polarized upon their conversion from P-to-S as they re-enter the mantle from the core. If these waves are split due to seismic anisotropy, energy will be visible on the transverse component. The transverse component $T(t)$ has the shape of the radial component time derivative $R'(t)$ if the wave is split due to seismic anisotropy (e.g., Silver & Chan, 1991; Vinnik et al., 1989). Furthermore, the transverse component amplitude reflects the strength of splitting affecting a particular waveform. Therefore, a quantity that characterizes shear-wave splitting of *KS waves is the splitting intensity (SI; Chevrot, 2000), which can be expressed as:

$$SI = -2\frac{T(t)R'(t)}{|R'(t)|^2}. \quad (1)$$

Previous work has shown that splitting intensity is a particularly convenient measurement for *KS splitting discrepancy studies (e.g., Deng et al., 2017; Reiss et al., 2019). We determine the splitting intensity of SKS,

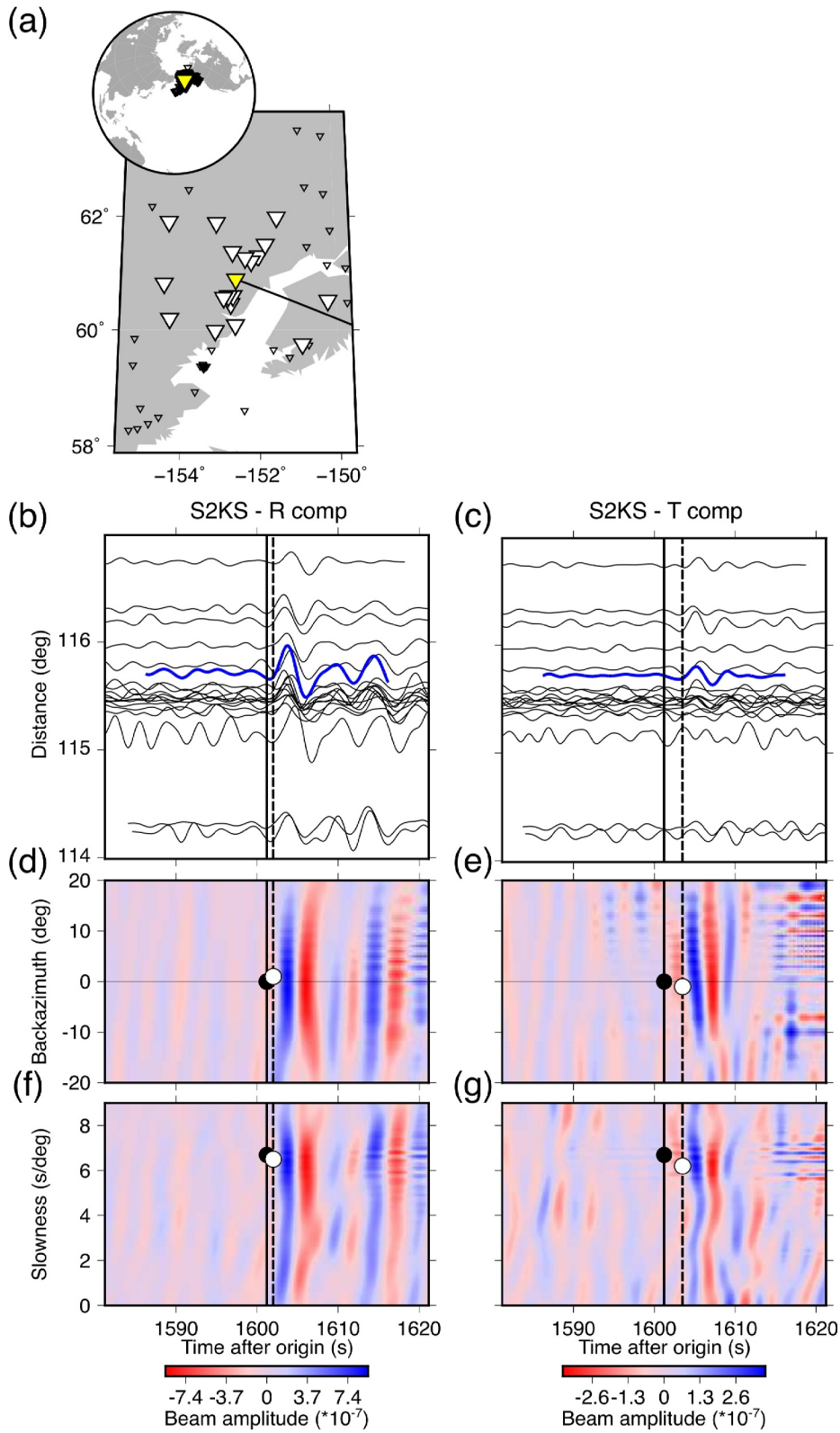

Figure 2.

S2KS, S3KS, and PKS (Figure 1b, inset) beams using SplitRacer (Reiss & Rümpker, 2017), a MATLAB toolkit to compute shear-wave splitting. To ensure the robustness of our *SI* measurements, we repeat them for 30 randomly selected time windows for most phases and only include results that are consistent across all time windows. For S3KS, we manually select the time window because this phase often arrives shortly after S2KS, which renders the automatic time window selection impractical. We always bandpass-filter our beams to retain periods between 6 and 25 s, and only include measurements for beam waveforms with amplitudes at least twice as large as the noise level.

Example S2KS, S3KS, and PKS waveforms and *SI* measurements are shown in Figure 3. In this case, PKS is split only slightly ($SI \approx 0.3$), whereas S2KS and S3KS are split strongly ($SI \geq 0.9$). This differential splitting is likely due to the different raypaths of PKS compared to S2KS/S3KS through D″, while S2KS and S3KS are relatively similar (Figure 1b, inset). In general, differentially split *KS phase pairs with $\delta SI > 0.4$ indicate the presence of D″ anisotropy influencing shear-wave splitting of one phase more strongly than the other. In contrast, nondiscrepant splitting may often be due to weak or absent D″ anisotropy, although it can also be consistent with certain D″ anisotropy configurations (Tesoniero et al., 2020; Wolf et al., 2022).

In this study, we specifically focus on SKS-S2KS, SKS-S3KS, and PKS-S2KS differential beam splitting (e.g., the difference of *SI* values in Figure 3). The reason that we do not focus on differential beam splitting between S2KS-S3KS and PKS-SKS pairs is their similar raypaths at certain epicentral distances (Figure 1b, inset; Figure 4b). Figure 4 shows differential S2KS-S3KS and PKS-SKS beam splitting as a function of source-receiver distance and deep mantle raypath separation. For larger distances, receiver-side mantle raypaths of PKS and SKS become more similar (Figure 4a). Accordingly, absolute δSI-values tend to be lower at large distances, while the opposite is true for S2KS-S3KS (Figure 4b). This test is made possible by the use of beamformed data, which enables us to measure shear-wave splitting for many different *KS phases from the same seismogram.

3. Results and Discussion

3.1. Lowermost Mantle Anisotropy

We obtain ∼2500 measurements of differential SKS-S2KS splitting, ∼400 measurements of differential SKS-S3KS splitting, and ∼250 measurements of differential PKS-S2KS splitting. Binned differential splitting intensities (bin size 1.5° × 1.5°) between *KS pairs are presented in Figure 5, while Figure S1 in Supporting Information S1 shows individual measurements. The plotting convention is such that *SI* differences are projected laterally to the middle of the horizontal distance (viewed from above) between *KS pierce points (Figure 5a, inset) at the CMB and the top of the D″ layer. SKS-S2KS pairs, for example, can be affected by seismic anisotropy in D″ anywhere between the point where SKS pierces through the CMB and the point where S2KS leaves D″, which we assume is 250 km above the CMB for the purpose of this plotting convention. The line in between these two pierce points, viewed from above, we will refer to as the pierce point connecting segment (cyan line in Figure 5a, inset). We document large *KS splitting intensity differences, indicating the presence of D″ anisotropy, beneath the Bering Sea, the northeastern Pacific Ocean, the western/central United States, and western Canada. For ∼60 % of the beams, S2KS and/or S3KS are more strongly split than SKS or PKS; however, the opposite is true for some regions, including for SKS waves that sample the lowermost mantle beneath the northeastern Pacific Ocean and parts of the Bering Sea.

For each bin, we calculate differential *SI* averages considering all pierce point connecting segments crossing the bin (Figure 6a). We undertake this exercise because the (commonly used) plotting convention in Figure 5 can be

Figure 2. Illustration of the beamforming approach for an event that occurred on 29 September 2019. (a) Stations are represented as large white triangles if belonging to the selected subarray and as small black triangular outlines otherwise. The subarray is located in Southern Alaska (see inset) and its center (yellow triangle) is west of Anchorage. The incoming backazimuth of the wave is shown by the black line. (b) Radial and (c) transverse velocity traces recorded at the 18 stations are aligned on S2KS and normalized to the maximum across all traces and components. Vespagrams for (d, f) radial and (e, g) transverse components show beam amplitude as a function of (d, e) backazimuth and (f, g) slowness (y-axis) and time (x-axis). The PREM-predicted arrival time and slowness of each phase are marked by the solid black vertical line and black circle, respectively. The slowness that produces the maximum beam amplitude is marked at the time of maximum by the white circle, and the arrival time of this phase is marked by the dashed black vertical line. The blue traces in (b) and (c) shows the beam constructed using the slownesses marked by the white circles.

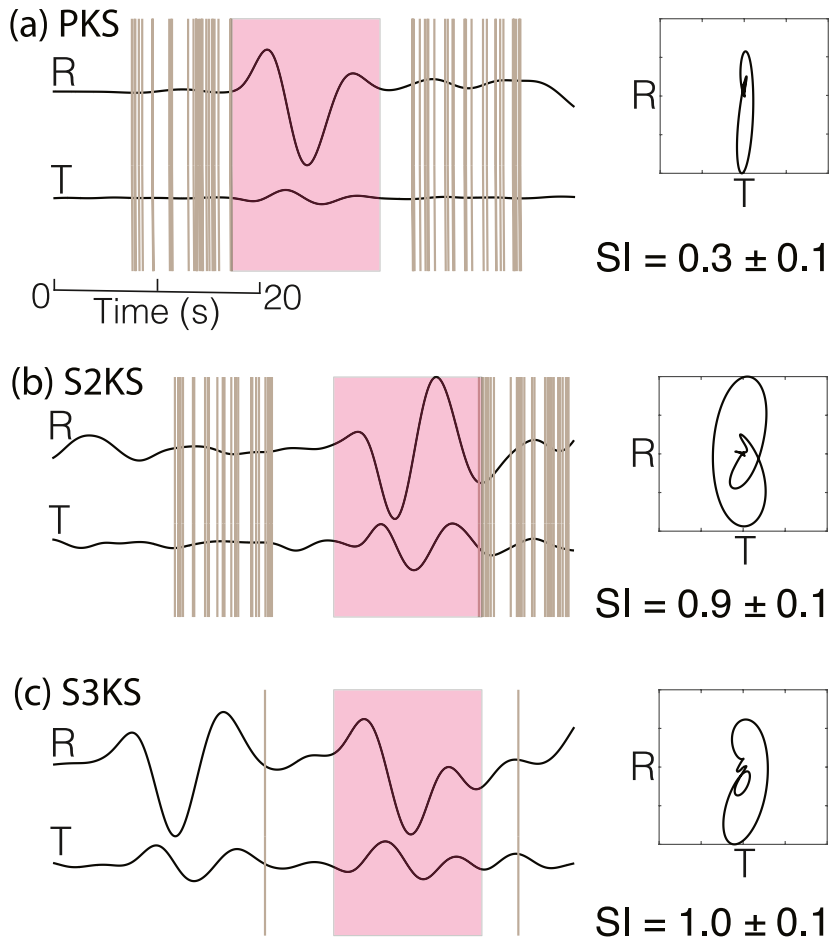

Figure 3. S2KS, S3KS, and PKS beamformed traces (velocity seismograms) and splitting intensity measurements for an event that occurred on 2 September 2009 in Java, Indonesia, and was recorded at a subarray with central station I20A, located in Wyoming at an epicentral distance of ∼132°. Waveforms were Hilbert-transformed to have the same phase as SKS. (a) Left: PKS radial (R) and transverse (T) waveforms (black lines). The amplitude of T is scaled to that of R which has been normalized to unity. Pink shading indicates the phase arrival, and vertical gray lines show start/end points of randomly selected time windows for *SI* analyses. Right: Particle motion plot (for the pink shaded region), showing transverse (x-axis) versus radial (y-axis) amplitude. Estimated *SI* with 95% confidence intervals are shown below. (b) Same as panel (a) for S2KS. (c) Same as panel (a) for S3KS. Note that for S3KS the analysis time window is manually selected to avoid interference with S2KS, which arrives just before S3KS. S2KS and S3KS *SI* measurements are similar (likely due to their similar raypaths through the mantle) and discrepant with PKS. For this example, we do not obtain a high-quality SKS beam.

misleading, as it only projects splitting intensity differences to a single point and does not consider the lengths of the pierce point connecting segments. For each bin, we expect a certain spread of values, because (a) the start/end points of different connecting segments differ, (b) shear wave splitting depends on the sampling angle of the seismic anisotropy, and (c) SKS and S2KS waves have different propagation directions through D″. Maximum standard deviations of the mean can be relatively high (up to ∼0.8) for some portions of our study area (Figure 6c). Elevated standard deviations in these areas are likely explained by different sampling angles of the seismic anisotropy and the presence of small-scale heterogeneity. We also calculate the percentage of connecting segments crossing each bin for which $|\delta SI|$ measurements >0.4 (Figure 6d).

We select a threshold of $|\delta SI| > 0.4$ (Figure 6d), in line with previous work suggesting that for individual splitting measurements this threshold can distinguish effects from lowermost mantle anisotropy from other influences, such as the upper mantle contributions due to slightly different raypaths (Tesoniero et al., 2020). However, it is worth emphasizing that this threshold applies to individual measurements, implying that when measurements are binned and averaged, even smaller $|\delta SI|$ values may be indicative of lowermost mantle anisotropy. The main

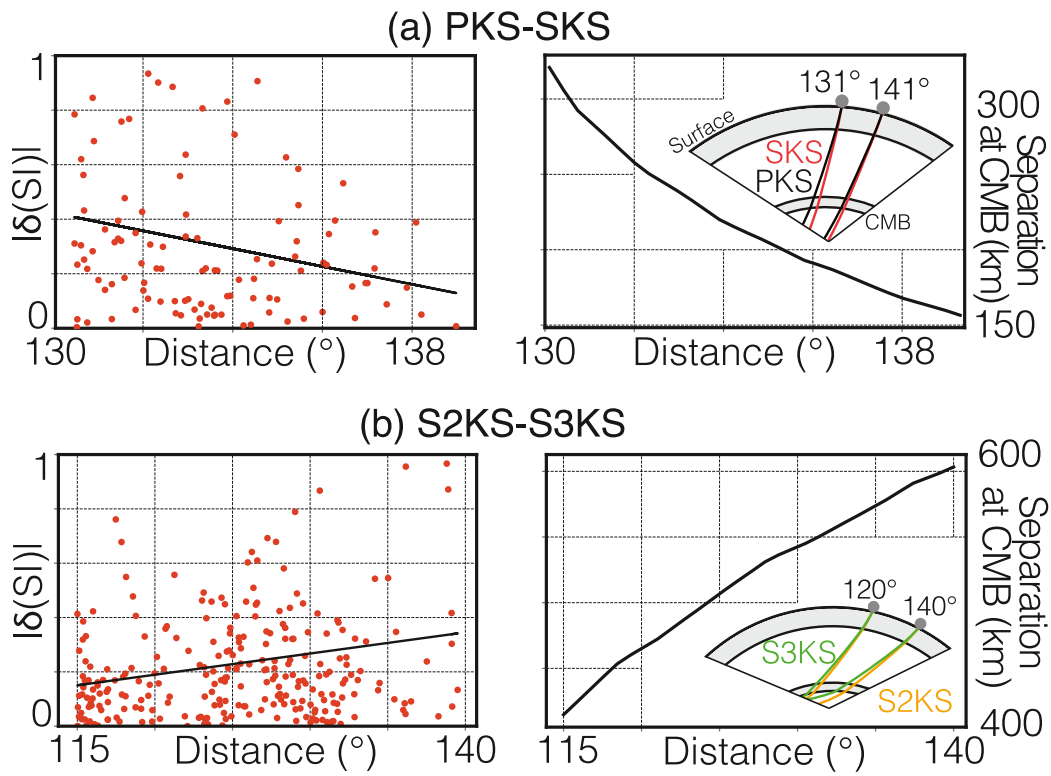

Figure 4. Splitting intensity differences between *KS phase pairs, whose differential splitting is not necessarily evidence for lowermost mantle anisotropy due to similar raypaths through the mantle at certain distances. (a) Left: $|\delta SI|$ values (red dots) for PKS and SKS, and least squares fit (black line) as a function of epicentral distance. Right: PKS-SKS raypath separation (black line) along the core-mantle boundary (CMB) as a function of epicentral distance. Inset: Cross-section through Earth showing of SKS (red) and PKS (black) raypaths. The (possibly anisotropic) upper and lowermost mantle are shown with gray shaded colors. $|\delta SI|$-values tend to be lower for larger distances, likely due to the smaller PKS-SKS raypath separation in the lowermost mantle at lower distances. (b) Same as panel (a) for S2KS-S3KS differential splitting. $|\delta SI|$-values tend to be higher for larger distances, likely due to the larger S2KS-S3KS raypath separation in the lowermost mantle at these distances.

reason is that for every lowermost mantle bin, $|\delta SI|$ values are recorded across different stations above a variably anisotropic (or isotropic) upper mantle. Therefore, effects from upper mantle anisotropy contributions may be unsystematic. Any averaged, unsystematic effects from upper mantle anisotropy contributions will have a lesser influence on the measurements as the number of contributing measurements in the bin increases.

Our view of data in Figure 6d helps us to distinguish four broad anisotropic regions. Region #1 covers the lowermost mantle beneath the Bering Sea, where seismic anisotropy has been identified in several previous shear-wave splitting studies (e.g., Garnero & Lay, 1997; Lay & Young, 1991; Matzel et al., 1996; Wysession et al., 1999). These previous studies all used ScS or S_{diff} waves that are sensitive to D″ anisotropy along long raypaths through D″. Our results using SKS-S2KS differential splitting confirm these findings with an independent method that is better suited to determine the lateral boundaries of the anisotropy due to the more nearly vertical raypaths of *KS phases through D″. The most detailed previous lateral and depth resolution of seismic anisotropy in Region #1 has been obtained by Suzuki et al. (2021). These authors inverted waveforms around the ScS arrivals for radially anisotropic structure, which is hard to explicitly compare with our shear-wave splitting measurements. The general result of strong seismic anisotropy, however, agrees. The study of Suzuki et al. (2021) suggests a geodynamic scenario in which upwellings form at the edges of approximately horizontally oriented slabs.

D″ anisotropy in parts of Region #2, which covers portions of D″ beneath the northeastern Pacific Ocean and western Canada, has been detected in previous work (e.g., Asplet et al., 2020, 2023; Wolf & Long, 2022; Wolf, Long, Creasy, & Garnero, 2023). Seismic anisotropy in this region has been interpreted as potentially caused by

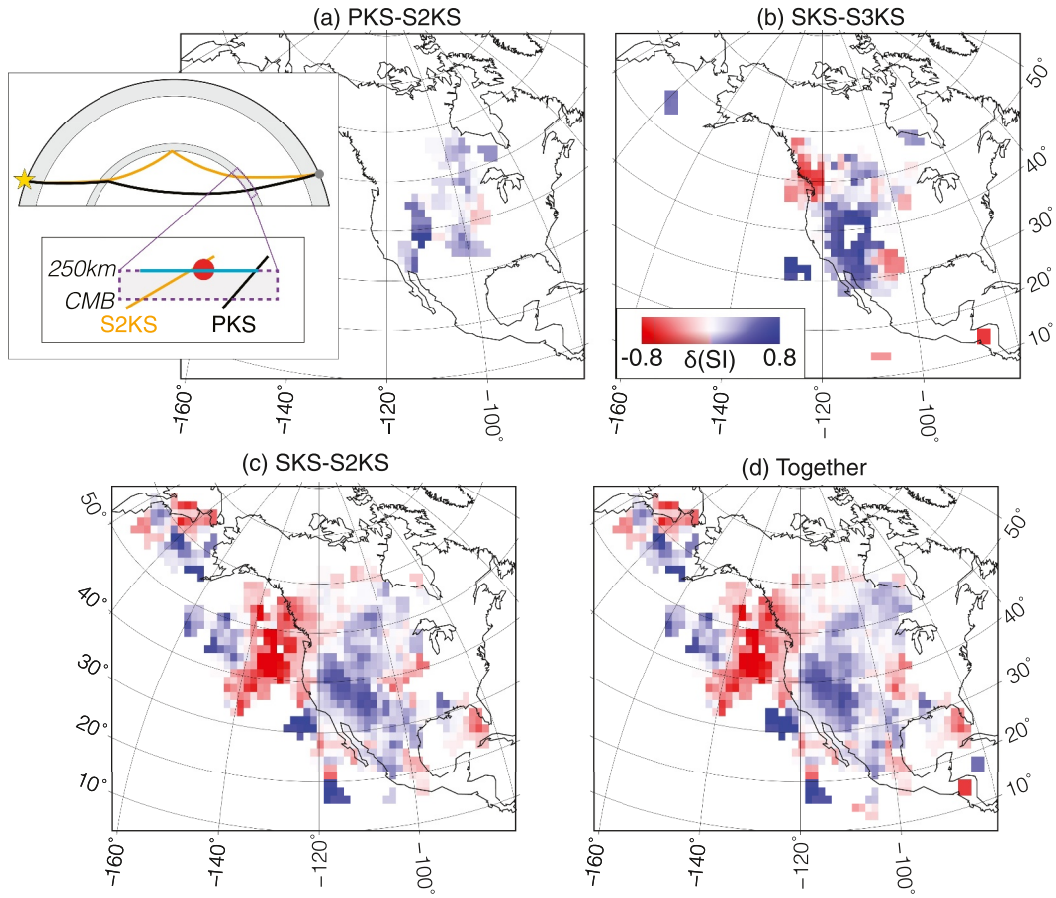

Figure 5. Binned (bin size 1.5° × 1.5°) splitting intensity differences between *KS phase pairs. (a) PKS minus S2KS splitting intensities (see legend). Values are positive if PKS *SI* values are greater than S2KS *SI* values and negative (or zero) otherwise. *SI* differences are projected laterally to the mid point between the S2KS pierce point through the CMB and the PKS pierce point 250 km above the CMB, as shown in the inset. Measurements are thus binned at the middle of the line that marks the ray-theoretical PKS-S2KS lowermost mantle sensitivity. Inset: Explanation of plotting convention. Top: S2KS (yellow) and PKS raypaths from source (yellow star) to receiver (gray circle) through an Earth cross-section. The upper mantle and D″ are shaded gray. Bottom: Zoom-in to the D″ region. Splitting intensities (red circle) are plotted in the middle of the S2KS-PKS pierce point connecting segment (cyan line). (b) Same as panel (a) for SKS-S3KS. (c) Same as panel (a) for SKS-S2KS. (d) Same as panel (a) for all measurements shown in panels (a)–(c).

crystallographic preferred orientation of post-perovskite crystals (Asplet et al., 2020, 2023), perhaps induced by slab-driven mantle flow (Wolf, Li, & Long, 2024; Wolf & Long, 2022).

Region #3 (Figure 6d) covers parts of the northeastern Pacific Ocean and large portions of the western and central United States. Previous studies that have found seismic anisotropy in parts of this region (e.g., Asplet et al., 2020, 2023; Lutz et al., 2020; Nowacki et al., 2010; Wolf, Li, Haws, & Long, 2024) have connected their findings to, for example, approximately horizontal flow along the CMB in large parts of Region #3 (e.g., Asplet et al., 2020; Nowacki et al., 2010), or to vertical flow at the Yellowstone plume root (Nelson & Grand, 2018) beneath Baja California (Wolf, Li, Haws, & Long, 2024). None of these studies, however, imaged the full broad extent of the anisotropic region that is shown in Figure 6d.

Seismic anisotropy in Region #4, to the west of the Mexican coast, has previously been inferred by Long (2009) through differential SKS-S2KS measurements. The precise lateral extent of this anisotropic region, however, remains unclear because it is located at the edge of our study region. Apart from the prominent Regions #1–4 that we highlight, the presence of seismic anisotropy is indicated in several places at the edge our study region. Due to the unknown spatial extent of these regions and the limited ray coverage within them (Figure 6b), we do not

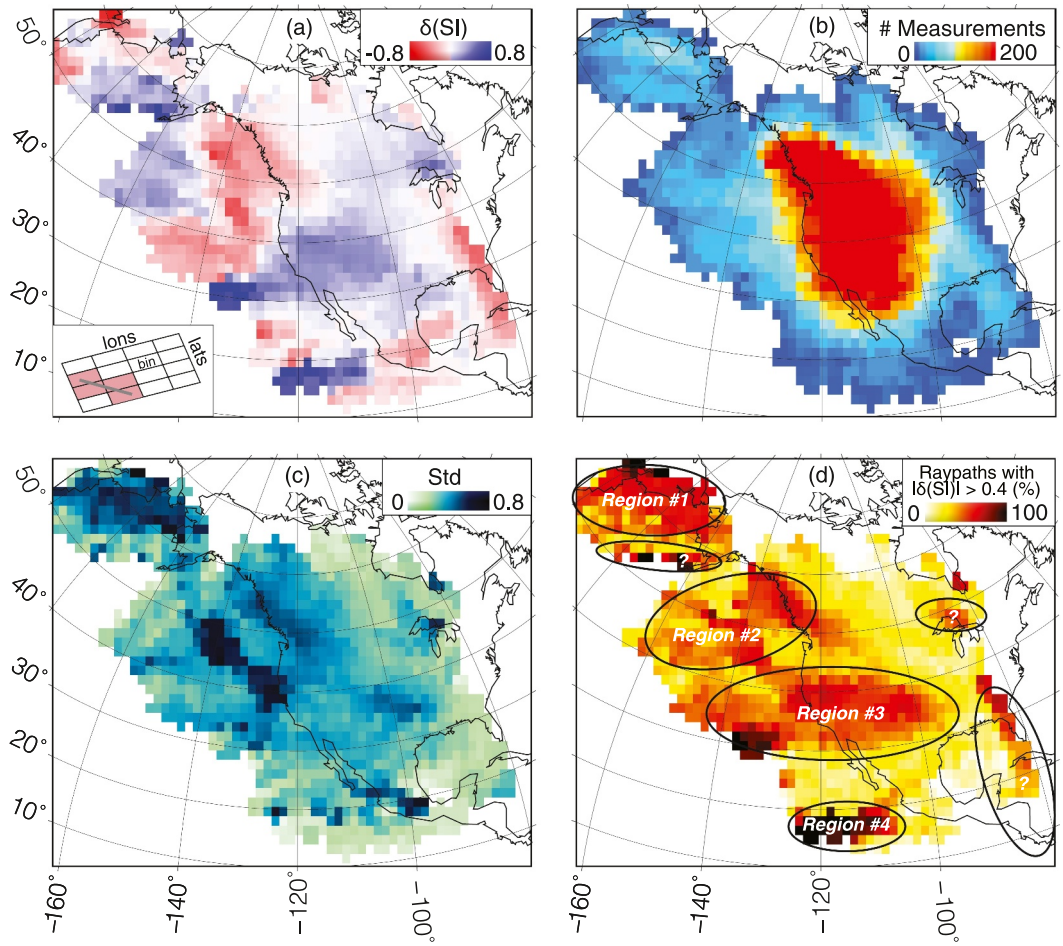

Figure 6. Measurement results considering pierce point connecting segments (see text and Figure 5a) crossing each bin. (a) δSI results for all seismic phase pairs shown in Figure 5 (see legend). Inset: pierce point connecting segment (gray) going through four bins (pink). The measurement is used for the average calculation in all pink bins. (b) Number of connecting segments (see legend) crossing each bin. (c) Standard deviations (see legend) of the averages shown in panel (a). (d) Percentage (see legend) of connecting segments (see text and Figure 5) with $|\delta SI| > 0.4$ through each bin. Four anisotropic regions are identified, which are marked by black ellipses for better referencing in the text.

interpret seismic anisotropy in these regions more closely. However, our results appear to be an ideal starting point for more detailed future investigations.

Our results provide a comprehensive picture of *KS splitting discrepancies due to D″ anisotropy beneath North America and the northeastern Pacific Ocean. Many previous studies of D″ anisotropy in our study region have linked their observations to mantle flow driven by slab remnants (e.g., Asplet et al., 2020, 2023; Long, 2009; Nowacki et al., 2010; Suzuki et al., 2021; Wolf & Long, 2022) or to smaller-scale regional upwellings in the lowermost mantle (Suzuki et al., 2021; Wolf, Li, Haws, & Long, 2024). Considering that remnants of several slabs (e.g., the Beaufort, Wichita, Izanagi, Farallon, and Telkhina slabs) likely reside in the lowermost mantle beneath North America and parts of the Pacific Ocean (Suzuki et al., 2021; van der Meer et al., 2018), it is plausible that some of the anisotropy we observe is due to the deformation induced by them. On the other hand, not all regions with higher than average velocities in D″ necessarily represent remnants of material that has been subducted (geologically) recently. More generally, the overall patterns of seismic anisotropy represent evidence for widespread strain-induced seismic anisotropy at the base of the mantle, with deformation accommodated in the dislocation creep regime. This strain in turn can be due to gradients in flow at the mantle's lower horizontal boundary layer.

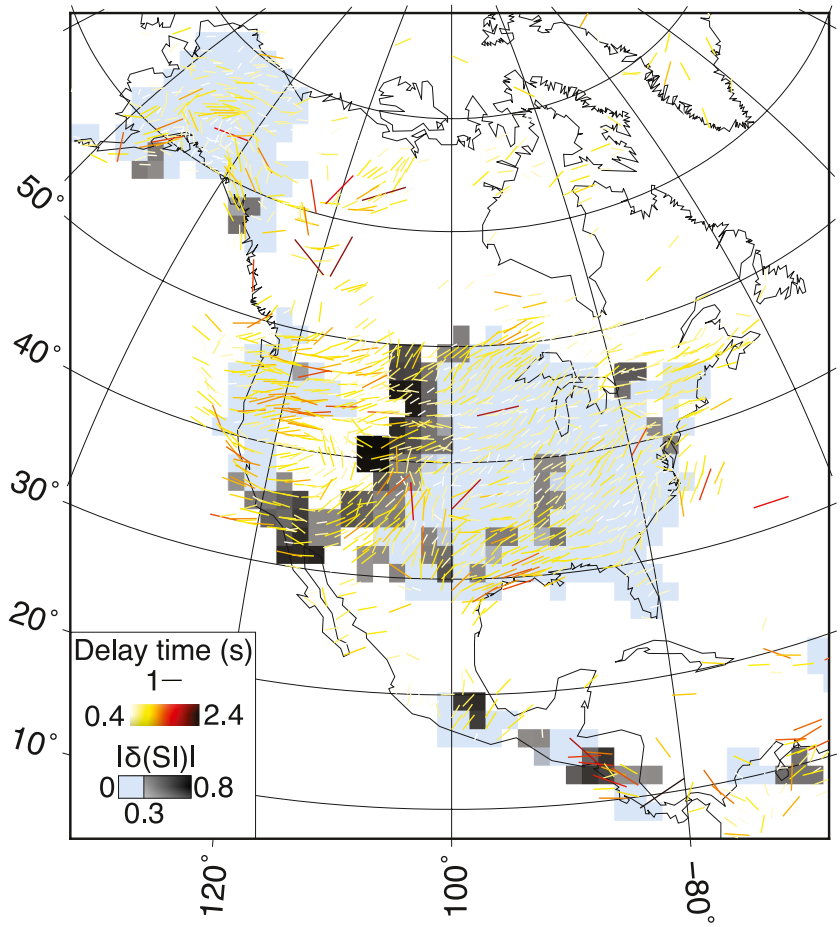

Figure 7. Potential influence of lowermost mantle anisotropy on upper mantle shear wave splitting measurements. Binned *KS *SI* differences projected to the station location are shown by the color scale. $|\delta SI|$-values <0.3 are shown in light blue, whereas larger values are shown by a gray scale (legend). We show 1° × 1° averages of delay times and fast polarization directions (colored sticks; see legend) from *KS (mostly SKS) splitting measurements compiled by Becker et al. (2012) and updated in December 2022.

3.2. Implications for Upper Mantle Anisotropy Studies

Tesoniero et al. (2020) and Wolf et al. (2022) have investigated in detail the possible influence of upper mantle seismic anisotropy on differential *KS measurements. The potential influence of D″ anisotropy on studies of upper mantle anisotropy relying on *KS splitting measurements, however, is not typically explicitly investigated. The reason is that upper mantle anisotropy is, on average, stronger than lowermost mantle anisotropy (Figure 1a); therefore, studies of upper mantle anisotropy typically assume that sufficiently accurate measurements of upper mantle splitting can be obtained without explicit consideration of the lowermost mantle splitting contribution. However, such an approach may not lead to precise results in all regions. The results of our study, based on high-SNR beamformed seismograms, enable an investigation of the potential influence of lowermost mantle anisotropy on *KS splitting measurements (which are typically interpreted as evidence for upper mantle anisotropy) across North and Central America.

Instead of projecting δSI values to their lowermost mantle location as in Figures 5–7, we show binned (bin size 1.5° × 1.5°) values at the subarray central station locations. Colored sticks in Figure 7 indicate shear wave splitting results from the updated compilation of Becker et al. (2012) that are often interpreted as being due to (mostly) upper mantle anisotropy. This database primarily relies on SKS splitting data. However, our differential *KS splitting results indicate that—in certain regions—the measured splitting may also be influenced by the lowermost mantle. It is worth noting that SKS-S2KS splitting intensity differences do not necessarily imply that, for example, SKS is influenced by D″ anisotropy and S2KS is not—and that the SKS splitting measurements,

therefore, partially reflect D″ anisotropy. More likely, in most cases, both SKS and S2KS splitting measurements are influenced by seismic anisotropy in the lowermost mantle. However, discrepant SKS-S2KS splitting in a particular station region implies that, without further information, measured splitting parameters cannot be confidently attributed to (only) upper mantle anisotropy. In some regions, in which SKS splitting is nearly null but SKKS is split, it is likely that a small number of SKS shear-wave splitting measurements have been previously reported in the literature. Such regions, with weak or absent SKS splitting, may have been implicitly excluded from previous upper mantle anisotropy analysis.

Averaged, binned *SI* differences across our station region can be as high as 0.8 (Figure 7). Given that delay times δt are mostly between 0.5 and 2 s across the United States (Liu et al., 2014; Yang et al., 2017) and the splitting intensity behaves approximately as $\delta t \sin[2(b-\phi)]$ (b = backazimuth; ϕ = fast polarization direction), this implies that the D″ contribution to *KS splitting is likely not negligible in all regions, as typically assumed. For example, Wolf, Li, Haws, and Long (2024) showed that SKS seismic waves recorded in southern California are strongly influenced by lowermost mantle anisotropy, likely accumulating absolute splitting intensities of ∼1.0 in D″, while S2KS likely is much less affected by seismic anisotropy in the deepest mantle in this region. Our results shown in Figure 7 are consistent with this finding, and indicate that more than half of the measured *SI* magnitudes in southern California, dependent on backazimuth, may be due to a D″ contribution. Additionally, in Montana, Wyoming and Colorado, *KS splitting measurements may be substantially affected by lowermost mantle seismic anisotropy (Figure 7). It has been argued that in this region effects of lowermost mantle anisotropy on S2KS are stronger than on SKS (Wolf & Long, 2022). However, the interpretations of upper mantle anisotropy in Montana, Wyoming and Colorado partly rely on S2KS splitting measurements (e.g., Yang et al., 2014), which may explain some of the inconsistent measurements of different previous studies (e.g., IRIS DMC, 2012; Liu et al., 2014). In addition to these two regions, *KS splitting recorded in parts of Ontario, Canada, and parts of Central America may be affected by a lowermost mantle anisotropy contribution (Figure 7). However, we obtain fewer measurements in these regions, which may mean that these results are less robust. Importantly, differential *KS splitting approach can reveal the backazimuthal directions from which the influence of lowermost mantle anisotropy may have to be considered. Our measurements in this study were mainly made using paths at backazimuths between −120° (Central America) and −30° (North America) (Figure 1b).

Our results in this study are based on measured splitting intensities. In studies of shear wave splitting due to upper mantle anisotropy, however, (ϕ, δt) measurements are used most frequently. If non-negligible lowermost mantle anisotropy is present and affecting shear-wave splitting measurements, which we have shown is the case in certain regions, (ϕ, δt) values used to infer upper mantle anisotropy will be affected in a non-trivial manner. To explicitly solve for the upper mantle contribution to splitting, essentially an inversion assuming two anisotropic layers is necessary (e.g., Bonnin et al., 2012; Silver & Savage, 1994). This issue may become even more challenging in cases in which more than one layer of seismic anisotropy may be present in the upper mantle.

Overall, our results indicate that the D″ contribution to *KS shear-wave splitting measurements is likely more important than often assumed, at least for some of the stations under study across the United States. There are several approaches that may be taken to ensure that splitting in studies of upper mantle anisotropy is indeed mainly due to an upper mantle anisotropy contribution. For example, nondiscrepant *KS splitting indicates that lowermost mantle anisotropy is unlikely to strongly influence splitting (although it could play a role for some specific anisotropy configurations). Moreover, our results reinforce the importance of measuring upper mantle shear-wave splitting for a range of backazimuths, as is often used to distinguish between simple or complex (e.g., Chen et al., 2018; Silver & Savage, 1994) seismic anisotropy. For example, if *SI* values as a function of backazimuth behave like a $\sin[2(b-\phi)]$-curve, splitting is likely due to upper mantle anisotropy. If there are deviations from such a pattern in a small backazimuthal window, a possible influence from D″ anisotropy on these measurements should be considered (e.g., Lynner & Long, 2012; Wolf, Li, Haws, & Long, 2024). Whether *KS differential splitting, backazimuthally varying splitting, or a combination of both approaches are used to distinguish effects from upper versus lowermost mantle anisotropy, beam splitting measurements are particularly helpful, as beamforming, by increasing SNRs, enables shear-wave splitting measurements for more phases and over larger backazimuthal and epicentral distance swaths than possible for single-station seismograms.

4. Conclusions

Using a large and comprehensive set of differential shear-wave splitting measurements from beamformed *KS data, we have identified evidence for widespread seismic anisotropy in four broad regions in the lowermost mantle beneath North America and the surrounding area. These regions encompass the base of the mantle beneath parts of the northern and eastern Pacific Ocean, the Bering Sea, western Canada, the United States, and part of Central America. The detected anisotropy is likely caused by mantle convection induced deformation, potentially linked in some larger regions to remnant slabs, and in more spatially restricted areas to upwelling flow. The detected D″ anisotropy likely has non-negligible effects on SKS splitting measurements for stations located in some regions across North and Central America, including southern California, Montana, Wyoming and Colorado as well as southeastern Ontario, Canada. Studies of upper mantle anisotropy using *KS waves should explicitly consider D″ contributions to shear-wave splitting, particularly for waves that travel through the lowermost mantle in regions that have previously been shown to be anisotropic, including our study region beneath North America.

Data Availability Statement

All data used in this study are publicly available through Earthscope (http://service.iris.edu/), NCEDC (https://ncedc.org/) (UC Berkeley Seismological Laboratory, 2014), SCEDC (https://scedc.caltech.edu/) (Caltech, 2014), SSN (http://www.ssn.unam.mx/) (Instituto de Geofísica, Universidad Nacional Autónoma de México, México, 2024), IPGP (http://ws.ipgp.fr/) (Institut de physique du globe de Paris (IPGP) & École et Observatoire des Sciences de la Terre de Strasbourg (EOST), 1982), GEOFON (https://geofon.gfz-potsdam.de/) (GFZ Data Services, 1993), and CNDC (https://www.earthquakescanada.nrcan.gc.ca/stndon/CNDC/index-en.php). Data were collected and pre-processed as part of ASU's global data collection system (http://adept.sese.asu.edu/) for their global record section project (http://swat.sese.asu.edu). We used data from networks 2T (Savvaidis, 2018b), 4O (Hodgkinson & Porritt, 2022), 4T (Savvaidis, 2018a), 6D (Carnegie Institute of Washington, 2009), 6J (Persaud, 2019), 7C (Schutt & Aster, 2015), 8G (Meltzer & Beck, 2016), AE (Arizona Geological Survey, 2007), AK (Alaska Earthquake Center, University of Alaska Fairbanks, 1987), AT (NOAA National Oceanic and Atmospheric Administration (USA), 1967), AV (Alaska Volcano Observatory/USGS, 1988), AY, AZ (UC San Diego, 1982), BC (Centro de Investigación Científica y de Educación Superior de Ensenada (CICESE), Ensenada, 1980), BR, C8, CI (California Institute of Technology and United States Geological Survey Pasadena, 1926), CM (Servicio Geológico Colombiano, 1993), CN (Natural Resources Canada (NRCAN Canada), 1975), CO (University of South Carolina, 1987), CU (Albuquerque Seismological Laboratory (ASL)/USGS, 2006), CW (National Centre for Seismological Research (CENAIS Cuba), 1998), CY, DE, DR (National Seismological Centre, 1998), EC, EO (University of Calgary, 2018), EP, GE (GEOFON Data Centre, 1993), G (Institut de physique du globe de Paris (IPGP) & École et Observatoire des Sciences de la Terre de Strasbourg (EOST), 1982), GI (Instituto Nacional de Sismologia, Vulcanologia, Meteorologia e Hidrologia (INSIVUMEH), 1976), GL (Institut De Physique Du Globe De Paris (IPGP), 2020a), GM (U.S. Geological Survey, 2016), GS (Albuquerque Seismological Laboratory (ASL)/USGS, 1980), IG, II (Scripps Institution of Oceanography, 1986), IM (Various Institutions, 1965), IU (Albuquerque Seismological Laboratory/USGS, 2014), MC, MG (Centro de Geociencias, UNAM, 2003), MQ (Institut De Physique Du Globe De Paris (IPGP), 2020b), MX (Red Sísmica Mexicana, 1970), N4 (Albuquerque Seismological Laboratory/USGS, 2013), NA (KNMI, 2006), NX (Nanometrics Seismological Instruments, 2013), NU (Instituto Nicaraguense de Estudios Territoriales (INETER), 1975), NY (University of Ottawa, 2013), OV (Obsercatorio Vulcanológico y Sismológico de Costa Rica, Universidad Nacional, 1984), PA (Red Sismica Volcan Baru, 2000), PQ (Geological Survey of Canada, 2013), PR (University of Puerto Rico, 1986), SC (New Mexico Tech, 1999), SS (Incorporated Research Institutions For Seismology, 1970), SV, TA (IRIS Transportable Array, 2003), TC (Universidad de Costa Rica, 2016), (Bureau of Economic Geology, The University of Texas at Austin, 2016), US (Albuquerque Seismological Laboratory (ASL)/USGS, 1990), WC, WI (Institut De Physique Du Globe De Paris (IPGP), 2008), XI (James, 2018), XO (Pavlis & Gilbert, 2011), XV (Wysession et al., 2011), YC (Truffer, 2021), YG (Christensen & Abers, 2016), YO, YU (Sell et al., 2006), Z7 (Klinglesmith, 2008), ZB (Velasco & Karplus, 2017), ZC (Pulliam, 2013), ZE (Tape et al., 2015), ZQ (Winberry et al., 2015), and ZW (DeShon et al., 2013). All beams used in this study are available at https://doi.org/10.5281/zenodo.12739753 (Wolf, Frost, et al., 2024). *Software availability*: SplitRacer (Reiss & Rümpker, 2017)

is publicly available at https://www.geophysik.uni-frankfurt.de/64002762/Software. All other codes/software used in this study are available at https://doi.org/10.5281/zenodo.12739753 (Wolf, Frost, et al., 2024).

Acknowledgments
This work was funded by Yale University, by the Miller Institute for Basic Science at UC Berkeley, and by the U.S. National Science Foundation via Grants EAR-2026917 to MDL, EAR-2027181 to DAF and EAR-1853911 to EG. The Generic Mapping Tools (Wessel & Smith, 1998) were used to create some of the figures and the TauP toolkit (Crotwell et al., 1999) was used for travel time computations. We are grateful to the reviewers Joseph Asplet and David Schlaphorst for their constructive comments that helped us improve the manuscript.

References

Alaska Earthquake Center, University of Alaska Fairbanks. (1987). Alaska geophysical network [Dataset]. https://doi.org/10.7914/SN/AK
Alaska Volcano Observatory/USGS. (1988). Alaska volcano observatory [Dataset]. https://doi.org/10.7914/SN/AV
Albuquerque Seismological Laboratory (ASL)/USGS. (1980). US geological survey networks [Dataset]. https://doi.org/10.7914/SN/GS
Albuquerque Seismological Laboratory (ASL)/USGS. (1990). United States national seismic network [Dataset]. https://doi.org/10.7914/SN/US
Albuquerque Seismological Laboratory (ASL)/USGS. (2006). Caribbean network [Dataset]. https://doi.org/10.7914/SN/CU
Albuquerque Seismological Laboratory/USGS. (2013). Central and eastern US network [Dataset]. https://doi.org/10.7914/SN/N4
Albuquerque Seismological Laboratory/USGS. (2014). Global seismograph network (GSN—IRIS/USGS) [Dataset]. https://doi.org/10.7914/SN/IU
Arizona Geological Survey. (2007). Arizona broadband seismic network [Dataset]. https://doi.org/10.7914/SN/AE
Asplet, J., Wookey, J., & Kendall, M. (2020). A potential post-perovskite province in D″ beneath the Eastern Pacific: Evidence from new analysis of discrepant SKS–SKKS shear-wave splitting. *Geophysical Journal International*, *221*(3), 2075–2090. https://doi.org/10.1093/gji/ggaa114
Asplet, J., Wookey, J., & Kendall, M. (2023). Inversion of shear wave waveforms reveal deformation in the lowermost mantle. *Geophysical Journal International*, *232*(1), 97–114. https://doi.org/10.1093/gji/ggac328
Becker, T. W., Lebedev, S., & Long, M. D. (2012). On the relationship between azimuthal anisotropy from shear wave splitting and surface wave tomography. *Journal of Geophysical Research*, *117*(B1), B01306. https://doi.org/10.1029/2011JB008705
Blandford, R. R. (1974). An automatic event detector at the Tonto Forest seismic observatory. *Geophysics*, *39*(5), 633–643. https://doi.org/10.1190/1.1440453
Bonnin, M., Tommasi, A., Hassani, R., Chevrot, S., Wookey, J., & Barruol, G. (2012). Numerical modelling of the upper-mantle anisotropy beneath a migrating strike-slip plate boundary: The San Andreas Fault system. *Geophysical Journal International*, *191*(2), 436–458. https://doi.org/10.1111/j.1365-246X.2012.05650.x
Bureau of Economic Geology, The University of Texas at Austin. (2016). Texas seismological network [Dataset]. https://doi.org/10.7914/SN/TX
California Institute of Technology and United States Geological Survey Pasadena. (1926). Southern California seismic network [Dataset]. https://doi.org/10.7914/SN/CI
Caltech. (2014). Southern California earthquake center [Dataset]. https://doi.org/10.7909/C3WD3xH1
Carnegie Institute of Washington. (2009). Telica seismic and deformation network [Dataset]. https://doi.org/10.7914/SN/6D_2009
Centro de Geociencias, UNAM. (2003). Permanent seismic network of Queretaro State, Mexico [Dataset]. https://doi.org/10.7914/SN/MG
Centro de Investigación Científica y de Educación Superior de Ensenada (CICESE), Ensenada. (1980). Red Sísmica del Noroeste de México [Dataset]. https://doi.org/10.7914/SN/BC
Chang, S.-J., Ferreira, A. M. G., Ritsema, J., van Heijst, H. J., & Woodhouse, J. H. (2015). Joint inversion for global isotropic and radially anisotropic mantle structure including crustal thickness perturbations. *Journal of Geophysical Research: Solid Earth*, *120*(6), 4278–4300. https://doi.org/10.1002/2014JB011824
Chen, X., Li, Y., & Levin, V. (2018). Shear wave splitting beneath eastern North American continent: Evidence for a multilayered and laterally variable anisotropic structure. *Geochemistry, Geophysics, Geosystems*, *19*(8), 2857–2871. https://doi.org/10.1029/2018GC007646
Chevrot, S. (2000). Multichannel analysis of shear wave splitting. *Journal of Geophysical Research*, *105*(B9), 21579–21590. https://doi.org/10.1029/2000JB900199
Christensen, D., & Abers, G. (2016). Fate and consequences of Yakutat terrane subduction beneath eastern Alaska and the Wrangell Volcanic Field [Dataset]. https://doi.org/10.7914/SN/YG_2016
Crotwell, P., Owens, T. J., & Ritsema, J. (1999). The TauP toolkit: Flexible seismic travel-time and raypath utilities. *Seismological Research Letters*, *70*(2), 154–160. https://doi.org/10.1785/gssrl.70.2.154
Deng, J., Long, M. D., Creasy, N., Wagner, L., Beck, S., Zandt, G., et al. (2017). Lowermost mantle anisotropy near the eastern edge of the Pacific LLSVP: Constraints from SKS-SKKS splitting intensity measurements. *Geophysical Journal International*, *210*(2), 774–786. https://doi.org/10.1093/gji/ggx190
DeShon, H., Hayward, C., Stump, B., Magnani, M. B., & Hornbach, M. (2013). North Texas earthquake study: Azle and Irving/Dallas [Dataset]. https://doi.org/10.7914/SN/ZW_2013
Dziewonski, A. M., & Anderson, D. L. (1981). Preliminary reference Earth model. *Physics of the Earth and Planetary Interiors*, *25*(4), 297–356. https://doi.org/10.1016/0031-9201(81)90046-7
French, S. W., & Romanowicz, B. A. (2014). Whole-mantle radially anisotropic shear velocity structure from spectral-element waveform tomography. *Geophysical Journal International*, *199*(3), 1303–1327. https://doi.org/10.1093/gji/ggu334
Frost, D. A., Garnero, E., Creasy, N., Wolf, J., Bozdag, E., Long, M., et al. (2024). Heterogeneous mantle effects on the behavior of SmKS waves and outermost core imaging. *Geophysical Journal International*, *237*(3), 1655–1673. https://doi.org/10.1093/gji/ggae135
Frost, D. A., Romanowicz, B., & Roecker, S. (2020). Upper mantle slab under Alaska: Contribution to anomalous core-phase observations on south-Sandwich to Alaska paths. *Physics of the Earth and Planetary Interiors*, *299*, 106427. https://doi.org/10.1016/j.pepi.2020.106427
Garnero, E. J., & Lay, T. (1997). Lateral variations in lowermost mantle shear wave anisotropy beneath the north Pacific and Alaska. *Journal of Geophysical Research*, *102*(B4), 8121–8135. https://doi.org/10.1029/96JB03830
GEOFON Data Centre. (1993). GEOFON seismic network [Dataset]. https://doi.org/10.14470/TR560404
Geological Survey of Canada. (2013). Public safety geoscience program Canadian research network [Dataset]. https://doi.org/10.7914/SN/PQ
GFZ Data Services. (1993). GEOFON data centre: GEOFON seismic network. https://doi.org/10.14470/TR560404
Hansen, L. N., Faccenda, M., & Warren, J. M. (2021). A review of mechanisms generating seismic anisotropy in the upper mantle. *Physics of the Earth and Planetary Interiors*, *313*, 106662. https://doi.org/10.1016/j.pepi.2021.106662
Hodgkinson, K., & Porritt, R. (2022). Sandia DAS [Dataset]. https://doi.org/10.7914/M8PY-H687
Incorporated Research Institutions For Seismology. (1970). Single station [Dataset]. https://doi.org/10.7914/SN/SS
Institut De Physique Du Globe De Paris (IPGP). (2008). GNSS, seismic broadband and strong motion permanent networks in West Indies [Dataset]. https://doi.org/10.18715/ANTILLES.WI
Institut De Physique Du Globe De Paris (IPGP). (2020a). Seismic, tiltmeter, extensometer, tide, magnetic and weather permanent networks on La Soufrière volcano and Guadeloupe [Dataset]. https://doi.org/10.18715/GUADELOUPE.GL

Institut De Physique Du Globe De Paris (IPGP). (2020b). Seismic, tiltmeter, groundwater, magnetic and weather permanent networks on Montagne Pelée volcano and Martinique [Dataset]. https://doi.org/10.18715/MARTINIQUE.MQ
Institut de physique du globe de Paris (IPGP)École et Observatoire des Sciences de la Terre de Strasbourg (EOST). (1982). GEOSCOPE, French global network of broad band seismic stations [Dataset]. https://doi.org/10.18715/GEOSCOPE.G
Instituto de Geofísica, Universidad Nacional Autónoma de México, México. (2024). Ssn: Servicio sismológico nacional [Dataset]. https://doi.org/10.21766/SSNMX/SN/MX
Instituto Nacional de Sismologia, Vulcanologia, Meteorologia e Hidrologia (INSIVUMEH). (1976). Red Sismologica Nacional [Dataset]. https://doi.org/10.7914/SN/GI
Instituto Nicaraguense de Estudios Territoriales (INETER). (1975). Nicaraguan seismic network [Dataset]. https://doi.org/10.7914/SN/NU
IRIS DMC. (2012). Data services products: SWS-DBs shear-wave splitting databases. https://doi.org/10.17611/DP/SWS.1
IRIS Transportable Array. (2003). USArray transportable array [Dataset]. https://doi.org/10.7914/SN/TA
James, S. (2018). Instrumentation for multidisciplinary monitoring of an Alaskan Peatland [Dataset]. https://doi.org/10.7914/SN/XI_2018
Karato, S.-I., Jung, H., Katayama, I., & Skemer, P. (2008). Geodynamic significance of seismic anisotropy of the upper mantle: New insights from laboratory studies. *Annual Review of Earth and Planetary Sciences*, *36*(1), 59–95. https://doi.org/10.1146/annurev.earth.36.031207.124120
Klinglesmith, D. (2008). MROI vibration studies [Dataset]. https://doi.org/10.7914/SN/Z7_2008
KNMI. (2006). Caribbean Netherlands seismic network [Dataset]. https://doi.org/10.21944/DFFA7A3F-7E3A-3B33-A436-516A01B6AF3F
Kocks, U., Tomé, C., & Wenk, H. (2000). *Texture and anisotropy: Preferred orientations in polycrystals and their effect on materials properties*. Cambridge University Press.
Lay, T., & Young, C. J. (1991). Analysis of seismic SV waves in the core's penumbra. *Geophysical Research Letters*, *18*(8), 1373–1376. https://doi.org/10.1029/91GL01691
Lin, Y.-P., Zhao, L., & Hung, S.-H. (2014). Full-wave effects on shear wave splitting. *Geophysical Research Letters*, *41*(3), 799–804. https://doi.org/10.1002/2013GL058742
Liu, K., Elsheikh, A., Lemnifi, A., Purevsuren, U., Ray, M., Refayee, H., et al. (2014). A uniform database of teleseismic shear wave splitting measurements for the western and central United States. *Geochemistry, Geophysics, Geosystems*, *15*(5), 2075–2085. https://doi.org/10.1002/2014GC005267
Long, M. (2009). Complex anisotropy in D″ beneath the eastern Pacific from SKS–SKKS splitting discrepancies. *Earth and Planetary Science Letters*, *283*(1–4), 181–189. https://doi.org/10.1016/j.epsl.2009.04.019
Long, M. D., & Becker, T. (2010). Mantle dynamics and seismic anisotropy. *Earth and Planetary Science Letters*, *297*(3–4), 341–354. https://doi.org/10.1016/j.epsl.2010.06.036
Lutz, K., Long, M. D., Creasy, N., & Deng, J. (2020). Seismic anisotropy in the lowermost mantle beneath North America from SKS-SKKS splitting intensity discrepancies. *Physics of the Earth and Planetary Interiors*, *305*, 106504. https://doi.org/10.1016/j.pepi.2020.106504
Lynner, C., & Long, M. D. (2012). Evaluating contributions to SK(K)S splitting from lower mantle anisotropy: A case study from station DBIC, Cote D'Ivoire. *Bulletin of the Seismological Society of America*, *102*(3), 1030–1040. https://doi.org/10.1785/0120110255
Matzel, E., Sen, M. K., & Grand, S. P. (1996). Evidence for anisotropy in the deep mantle beneath Alaska. *Geophysical Research Letters*, *23*(18), 2417–2420. https://doi.org/10.1029/96GL02186
Meade, C., Silver, P. G., & Kaneshima, S. (2005). Laboratory and seismological observations of lower mantle isotropy. *Geophysical Research Letters*, *22*(10), 1293–1296. https://doi.org/10.1029/95GL01091
Megnin, C., & Romanowicz, B. (2000). The shear velocity structure of the mantle from the inversion of body, surface and higher modes waveforms. *Geophysical Journal International*, *143*(3), 709–728. https://doi.org/10.1046/j.1365-246X.2000.00298.x
Meltzer, A., & Beck, S. (2016). 2016 Pedernales earthquake aftershock deployment Ecuador [Dataset]. https://doi.org/10.7914/SN/8G_2016
Montagner, J.-P. (1998). Where can seismic anisotropy be detected in the Earth's mantle? In boundary layers. In J. Plomerová, R. C. Liebermann, & V. Babuška (Eds.), *Geodynamics of lithosphere & Earth's mantle* (pp. 223–256).
Nanometrics Seismological Instruments. (2013). Nanometrics research network [Dataset]. https://doi.org/10.7914/SN/NX
National Centre for Seismological Research (CENAIS Cuba). (1998). Servicio Sismologico Nacional de Cuba [Dataset]. https://doi.org/10.7914/SN/CW
National Seismological Centre. (1998). Centro Nacional de Sismologia [Dataset]. https://doi.org/10.7914/SN/DR
Natural Resources Canada (NRCAN Canada). (1975). Canadian national seismograph network [Dataset]. https://doi.org/10.7914/SN/CN
Nelson, P. L., & Grand, S. P. (2018). Lower-mantle plume beneath the Yellowstone hotspot revealed by core waves. *Nature Geoscience*, *11*(4), 280–284. https://doi.org/10.1038/s41561-018-0075-y
New Mexico Tech. (1999). New Mexico tech seismic network [Dataset]. https://doi.org/10.7914/0ABK-1345
Niu, F., & Perez, A. M. (2004). Seismic anisotropy in the lower mantle: A comparison of waveform splitting of SKS and SKKS. *Geophysical Research Letters*, *31*(24). https://doi.org/10.1029/2004GL021196
NOAA National Oceanic and Atmospheric Administration (USA). (1967). National tsunami warning center Alaska seismic network [Dataset]. https://doi.org/10.7914/SN/AT
Nowacki, A., Wookey, J., & Kendall, J.-M. (2010). Deformation of the lowermost mantle from seismic anisotropy. *Nature*, *467*(7319), 1091–1094. https://doi.org/10.1038/nature09507
Obsercatorio Vulcanológico y Sismológico de Costa Rica, Universidad Nacional. (1984). Observatorio Vulcanológico y Sismológico de Costa Rica [Dataset]. https://doi.org/10.7914/SN/OV
Panning, M., & Romanowicz, B. (2006). A three-dimensional radially anisotropic model of shear velocity in the whole mantle. *Geophysical Journal International*, *167*(1), 361–379. https://doi.org/10.1111/j.1365-246X.2006.03100.x
Pavlis, G., & Gilbert, H. (2011). Ozark Illinois Indiana Kentucky (OIINK) flexible array experiment [Dataset]. https://doi.org/10.7914/SN/XO_2011
Persaud, P. (2019). Los Angeles basin seismic experiment [Dataset]. https://doi.org/10.7914/SN/6J_2019
Pulliam, J. (2013). Greater Antilles seismic program [Dataset]. https://doi.org/10.7914/SN/ZC_2013
Red Sísmica Mexicana. (1970). Mexican national seismic network [Dataset]. https://doi.org/10.21766/SSNMX/SN/MX
Red Sismica Volcan Baru. (2000). Chirinet [Dataset]. https://doi.org/10.7914/SN/PA
Reiss, M., & Rümpker, G. (2017). SplitRacer: MATLAB code and GUI for semiautomated analysis and interpretation of teleseismic shear-wave splitting. *Seismological Research Letters*, *88*(2A), 392–409. https://doi.org/10.1785/0220160191
Reiss, M. C., Long, M. D., & Creasy, N. (2019). Lowermost mantle anisotropy beneath Africa from differential SKS-SKKS shear-wave splitting. *Journal of Geophysical Research: Solid Earth*, *124*(8), 8540–8564. https://doi.org/10.1029/2018JB017160
Romanowicz, B., & Wenk, H.-R. (2017). Anisotropy in the deep Earth. *Physics of the Earth and Planetary Interiors*, *269*, 58–90. https://doi.org/10.1016/j.pepi.2017.05.005

Rost, S., & Thomas, C. (2002). Array seismology: Methods and applications. *Reviews of Geophysics*, *40*(3), 1–27. https://doi.org/10.1029/2000RG000100

Rost, S., & Thomas, C. (2009). Improving seismic resolution through array processing techniques. *Surveys in Geophysics*, *30*(4–5), 271–299. https://doi.org/10.1007/s10712-009-9070-6

Savage, M. K. (1999). Seismic anisotropy and mantle deformation: What have we learned from shear wave splitting? *Reviews of Geophysics*, *37*(1), 65–106. https://doi.org/10.1016/10.1029/98RG02075

Savvaidis, A. (2018a). Texas seismological network [Dataset]. https://doi.org/10.7914/SN/4T_2018

Savvaidis, A. (2018b). Texas temporary arrays [Dataset]. https://doi.org/10.7914/SN/2T_2018

Schutt, D., & Aster, R. (2015). The Mackenzie Mountains transect: Active deformation from margin to craton [Dataset]. https://doi.org/10.7914/SN/7C_2015

Scripps Institution of Oceanography. (1986). Global seismograph network—IRIS/IDA [Dataset]. https://doi.org/10.7914/SN/II

Selby, N. D. (2008). Application of a generalized F detector at a seismometer array. *Bulletin of the Seismological Society of America*, *98*(5), 2469–2481. https://doi.org/10.1785/0120070282

Sell, R., Fletcher, J., & Boatwright, J. (2006). Northern California delta [Dataset]. https://doi.org/10.7914/SN/YU_2006

Servicio Geológico Colombiano. (1993). Red Sismologica Nacional de Colombia [Dataset]. https://doi.org/10.7914/SN/CM

Sieminski, A., Paulssen, H., Trampert, J., & Tromp, J. (2008). Finite-frequency SKS splitting: Measurement and sensitivity Kernels. *Bulletin of the Seismological Society of America*, *98*(4), 1797–1810. https://doi.org/10.1785/0120070297

Silver, P. G., & Chan, W. W. (1991). Shear wave splitting and subcontinental mantle deformation. *Journal of Geophysical Research*, *96*(B10), 16429–16454. https://doi.org/10.1029/91JB00899

Silver, P. G., & Savage, M. K. (1994). The interpretation of shear-wave splitting parameters in the presence of two anisotropic layers. *Geophysical Journal International*, *119*(3), 949–963. https://doi.org/10.1111/j.1365-246X.1994.tb04027.x

Suzuki, Y., Kawai, K., & Geller, R. J. (2021). Imaging paleoslabs and inferring the Clapeyron slope in D″ beneath the northern Pacific based on high-resolution inversion of seismic waveforms for 3-D transversely isotropic structure. *Physics of the Earth and Planetary Interiors*, *321*, 106751. https://doi.org/10.1016/j.pepi.2021.106751

Tape, C., Christensen, D. H., & Moore-Driskell, M. M. (2015). Southern Alaska lithosphere and mantle observation network [Dataset]. https://doi.org/10.7914/SN/ZE_2015

Tesoniero, A., Leng, K., Long, M. D., & Nissen-Meyer, T. (2020). Full wave sensitivity of SK(K)S phases to arbitrary anisotropy in the upper and lower mantle. *Geophysical Journal International*, *222*(1), 412–435. https://doi.org/10.1093/gji/ggaa171

Truffer, M. (2021). Seismic monitoring of the Muldrow Surge [Dataset]. https://doi.org/10.7914/SN/YC_2021

UC Berkeley Seismological Laboratory. (2014). Northern California earthquake data center [Dataset]. https://doi.org/10.7932/NCEDC

UC San Diego. (1982). ANZA regional network [Dataset]. https://doi.org/10.7914/SN/AZ

Universidad de Costa Rica. (2016). Información de la Red Sismológica Nacional de Costa Rica [Dataset]. https://doi.org/10.15517/TC

University of Calgary. (2018). EON-ROSE [Dataset]. https://doi.org/10.7914/SN/EO

University of Ottawa. (2013). Yukon-northwest seismic network [Dataset]. https://doi.org/10.7914/SN/NY

University of Puerto Rico. (1986). Puerto Rico seismic network & Puerto Rico strong motion program [Dataset]. https://doi.org/10.7914/SN/PR

University of South Carolina. (1987). South Carolina seismic network [Dataset]. https://doi.org/10.7914/SN/CO

U.S. Geological Survey. (2016). U.S. geological survey networks [Dataset]. https://doi.org/10.7914/SN/GM

van der Meer, D. G., van Hinsbergen, D. J., & Spakman, W. (2018). Atlas of the underworld: Slab remnants in the mantle, their sinking history, and a new outlook on lower mantle viscosity. *Tectonophysics*, *723*, 309–448. https://doi.org/10.1016/j.tecto.2017.10.004

Various Institutions. (1965). International miscellaneous stations [Dataset]. https://doi.org/10.7914/VEFQ-VH75

Velasco, A., & Karplus, M. (2017). Rapid aftershock deployment for the September 2017 M=8.1 and M.7.1 earthquakes in Mexico (RADSEM) [Dataset]. https://doi.org/10.7914/SN/ZB_2017

Vinnik, L., Farra, V., & Romanowicz, B. (1989). Azimuthal anisotropy in the Earth from observations of SKS at GEOSCOPE and NARS broadband stations. *Bulletin of the Seismological Society of America*, *79*, 1542–1558. https://doi.org/10.1785/BSSA0790051542

Wang, Y., & Wen, L. (2004). Mapping the geometry and geographic distribution of a very low velocity province at the base of the Earth's mantle. *Journal of Geophysical Research*, *109*(B10), B10305. https://doi.org/10.1029/2003JB002674

Wenk, H.-R., & Houtte, P. V. (2004). Texture and anisotropy. *Reports on Progress in Physics*, *67*(8), 1367–1428. https://doi.org/10.1088/0034-4885/67/8/R02

Wessel, P., & Smith, W. H. F. (1998). New, improved version of generic mapping tools released. *Eos, Transactions American Geophysical Union*, *79*(47), 579. https://doi.org/10.1029/98EO00426

Winberry, P., Walter, J., Amundson, J., & Bartholomaus, T. (2015). Taku Glacier [Dataset]. https://doi.org/10.7914/SN/ZQ_2015

Wolf, J., Frost, D. A., Brewster, A., Long, M. D., Garnero, E., & West, J. D. (2024). Additional data/codes concerning "Widespread D″ anisotropy beneath North America and the northeastern Pacific and implications for upper mantle anisotropy measurements [Dataset]. *Zenodo*. https://doi.org/10.5281/zenodo.12739753

Wolf, J., Frost, D. A., Long, M. D., Garnero, E., Aderoju, A. O., Creasy, N., & Bozdag, E. (2023). Observations of mantle seismic anisotropy using array techniques: Shear-wave splitting of beamformed SmKS phases. *Journal of Geophysical Research: Solid Earth*, *128*(1), e2022JB025556. https://doi.org/10.1029/2022JB025556

Wolf, J., Li, M., Haws, A. A., & Long, M. D. (2024). Strong seismic anisotropy due to upwelling flow at the root of the Yellowstone mantle plume. *Geology*, *52*(5), 379–382. https://doi.org/10.1130/G51919.1

Wolf, J., Li, M., Long, M., & Garnero, E. (2024). Advances in mapping lowermost mantle convective flow with seismic anisotropy observations. *Reviews of Geophysics*, *62*(2), e2023RG000833. https://doi.org/10.1029/2023RG000833

Wolf, J., Li, M., & Long, M. D. (2024). Low-velocity heterogeneities redistributed by subducted material in the deepest mantle beneath North America. *Earth and Planetary Science Letters*, *642*, 118867. https://doi.org/10.1016/j.epsl.2024.118867

Wolf, J., & Long, M. D. (2022). Slab-driven flow at the base of the mantle beneath the northeastern Pacific Ocean. *Earth and Planetary Science Letters*, *594*, 117758. https://doi.org/10.1016/j.epsl.2022.117758

Wolf, J., & Long, M. D. (2023). Upper mantle anisotropy and flow beneath the Pacific Ocean revealed by differential PS-SKS splitting. *Geophysical Research Letters*, *50*(16), e2023GL104402. https://doi.org/10.1029/2023GL104402

Wolf, J., Long, M. D., Creasy, N., & Garnero, E. (2023). On the measurement of S_{diff} splitting caused by lowermost mantle anisotropy. *Geophysical Journal International*, *233*(2), 900–921. https://doi.org/10.1093/gji/ggac490

Wolf, J., Long, M. D., & Frost, D. A. (2024). Ultralow velocity zone and deep mantle flow beneath the Himalayas linked to subducted slab. *Nature Geoscience*, *17*(4), 1–7. https://doi.org/10.1038/s41561-024-01386-5

Wolf, J., Long, M. D., Leng, K., & Nissen-Meyer, T. (2022). Constraining deep mantle anisotropy with shear wave splitting measurements: Challenges and new measurement strategies. *Geophysical Journal International*, *230*(1), 507–527. https://doi.org/10.1093/gji/ggac055

Wolf, J., Long, M. D., Li, M., & Garnero, E. (2023). Global compilation of deep mantle anisotropy observations and possible correlation with low velocity provinces. *Geochemistry, Geophysics, Geosystems*, *24*(10), e2023GC011070. https://doi.org/10.1029/2023GC011070

Wysession, M. E., Langenhorst, A., Fouch, M. J., Fischer, K. M., Al-Eqabi, G. I., Shore, P. J., & Clarke, T. J. (1999). Lateral variations in compressional/shear velocities at the base of the mantle. *Science*, *284*(5411), 120–125. https://doi.org/10.1126/science.284.5411.120

Wysession, M. E., Wiens, D., & Nyblade, A. (2011). Investigation of sources of intraplate volcanism using PASSCAL broadband instruments in Madagascar, the Comores, and Mozambique [Dataset]. https://doi.org/10.7914/SN/XV_2011

Yang, B., Gao, S. S., Liu, K. H., Elsheikh, A. A., Lemnifi, A. A., Refayee, H. A., & Yu, Y. (2014). Seismic anisotropy and mantle flow beneath the northern Great Plains of North America. *Journal of Geophysical Research: Solid Earth*, *119*(3), 1971–1985. https://doi.org/10.1002/2013JB010561

Yang, B., Liu, Y., Dahm, H., Liu, K., & Gao, S. (2017). Seismic azimuthal anisotropy beneath the eastern United States and its geodynamic implications. *Geophysical Research Letters*, *44*(6), 2670–2678. https://doi.org/10.1002/2016GL071227